PCCP

View Online / Journal Homepage
Dynamic Article Links

Cite this: DOI: 10.1039/c2cp40740j

www.rsc.org/pccp

PAPER

Classical toy models for the monopole shift and the quadrupole shift

Katrin Rose†‡*[a] and Stefaan Cottenier‡*[b]

Received 8th March 2012, Accepted 28th May 2012
DOI: 10.1039/c2cp40740j

The penetration of s- and $p_{1/2}$-electrons into the atomic nucleus leads to a variety of observable effects. The presence of s-electrons inside the nucleus gives rise to the isotope shift in atomic spectroscopy, and to the isomer shift in Mössbauer spectroscopy. Both well-known phenomena are manifestations of the more general *monopole shift*. In a recent paper (Koch *et al.*, *Phys. Rev. A*, 2010, **81**, 032507), we discussed the existence of the formally analogous *quadrupole shift*: a tensor correction to the electric quadrupole interaction due to the penetration of relativistic $p_{1/2}$-electrons into the nucleus. The quadrupole shift is predicted to be observable by high-accuracy molecular spectroscopy on a set of 4 molecules (the *quadrupole anomaly*). The simple physics behind all these related phenomena is easily obscured by an elaborate mathematical formalism that is required for their derivation: a multipole expansion in combination with perturbation theory, invoking quantum physics and ideally relativity. In the present paper, we take a totally different approach. We consider three classical 'toy models' that can be solved by elementary calculus, and that nevertheless contain all essential physics of the monopole and quadrupole shifts. We hope that this intuitive (yet exact) analysis will increase the understanding about multipole shift phenomena in a broader community.

1 Introduction

The penetration of electrons into the volume of the nucleus leads to a variety of observable effects. Best known are the ones that are connected to the penetration of s-electrons into the nucleus: the isotope shift in atomic spectroscopy, and the isomer shift in Mössbauer spectroscopy. It is common practice to discuss these effects in terms of a multipole expansion in combination with perturbation theory, where s-electrons inside the nucleus manifest themselves mainly by the leading term in the "near-field" corrections. Albeit being mathematically convenient and quantitatively nearly exact for all common purposes, such a discussion obscures the simple physics that is behind. This is even more true when it comes to the penetration of relativistic $p_{1/2}$-electrons into the nucleus: as this leads to a tensor correction (rank 2) rather than to a scalar correction, an intuitive understanding of the physics is even more remote. The consequences of $p_{1/2}$-penetration were pointed out for the first time 40 years ago,[1] but have only recently been discussed in detail.[2–6] The size of the effect is very small, and experimental observation – predicted to be possible under the form of a so-called "quadrupole anomaly"[6] – is still being attempted for.

The aim of the present work is to highlight the physics behind both s- and $p_{1/2}$-penetration, without resorting to a heavy mathematical formalism nor to quantum physics. We will discuss three 'toy models': configurations of positive and negative classical charges that are so simple that their interaction energy can be calculated exactly, using no math that goes beyond the level of an introductory course in classical electrostatics. The properties of these models are sufficient to demonstrate the essential physics of the isotope shift, isomer shift, quadrupole shift and quadrupole anomaly (Sections 2–5). The target audience for this analysis are in the first place scientists from the molecular spectroscopy community (who have the tools for observing the new quadrupole anomaly), as well as scientists from the atomic spectroscopy, Mössbauer and hyperfine communities (who have a tradition on monopole shift phenomena). It is our hope that such an alternative and intuitive approach to these properties will increase the general understanding about them in a broader community.

2 Toy models: tm0 and tmA

2.1 A toy nucleus

Throughout this paper, we will use the charge distribution that is shown in Fig. 1(a) as a classical analog for a nucleus. It consists of two positive point charges $+e$, connected by a rigid rod of length 2ℓ. This 'nucleus' is fixed with its center of charge (the middle of the rod) at the origin of an XYZ axis system, and can freely rotate about this fixed point. The angles θ and ϕ

[a] *DAHO, Heerlener Straße 26, DE-52074 Aachen, Germany. E-mail: KatrinRose79@googlemail.com*
[b] *Center for Molecular Modeling & Department of Materials Science and Engineering, Ghent University, Technologiepark 903, BE-9052 Zwijnaarde, Belgium. E-mail: Stefaan.Cottenier@ugent.be*
† Formerly named Katrin Koch.
‡ These authors contributed equally to this work.

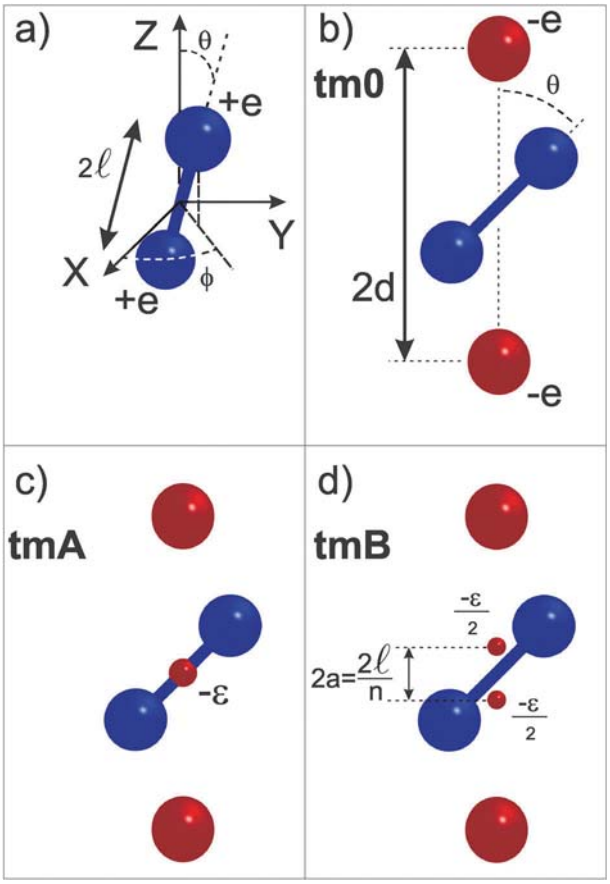

Fig. 1 The toy models that are discussed in this work: (a) the model for the toy nucleus: a nuclear dumb-bell consisting of two positive point charges connected by a rigid rod. (b) tm0: the nuclear dumb-bell in the field of two fixed point charges, without electron penetration into the nucleus. (c) tmA: same as tm0, but now with a spherical electron distribution inside the nuclear volume. (d) tmB: same as tm0, but now with a non-spherical electron distribution inside the nuclear volume, *i.e.* two point charges.

(see Fig. 1(a)) define the absolute orientation of the nucleus in space.

2.2 Electrons outside the nucleus: tm0

We put the toy nucleus into a given negative charge distribution, which consists of two negative point charges $-e$ that are fixed at a distance d along the positive and negative Z-axis. The combination of this particular negative charge distribution ('the electron cloud') and the toy nucleus, we call *toy model* 0 (tm0). It is drawn in Fig. 1(b). What distinguishes tm0 from the other two toy models, which will be discussed later, is that for any orientation of the nucleus, there will never be negative (electron) charges inside the nuclear volume.

The key property which we want to determine for tm0 and any of the later toy models, is the electrostatic interaction energy between the 'nucleus' and the 'electrons', as a function of the orientation of the nucleus: $E_0(\theta,\phi)$. It follows readily from symmetry considerations that this energy for tm0 depends only on θ: $E_0(\theta)$ (the distance between the positive and negative point charges does not change upon rotating the nucleus while keeping the inclination with respect to the Z-axis fixed).

Straightforward application of Coulomb's law leads to the following expression ($\ell < d$ is assumed):

$$E_0(\theta) = -2C\left(\frac{1}{\sqrt{\ell^2\sin^2\theta + (d-\ell\cos\theta)^2}} + \frac{1}{\sqrt{\ell^2\sin^2\theta + (d+\ell\cos\theta)^2}}\right). \quad (1)$$

The positive constant C will appear many times hereafter, and has the value $C = e^2/(4\pi\varepsilon_0)$. It is more instructive to examine a graphical representation of eqn (1) (Fig. 2): the interaction energy is always negative, indicating that the system is bound. $E_0(\theta)$ is the energy that is required to translate the nucleus to an infinite distance from the electrons. The lowest energy state of the system is obtained when the nucleus lies parallel to the Z-axis ($\theta_{min} = 0^\circ$ or $\theta_{min} = 180^\circ$). The energy is maximal for the nucleus lying in the XY-plane ($\theta_{max} = 90^\circ$). Depending on the orientation of the nucleus, any energy between these two extrema can be reached. This distinguishes this classical case from the quantum case, where only discrete orientations and therefore only discrete energies are allowed.

We will characterize the behaviour expressed by eqn (1) by two numbers: the average interaction energy E_{av} and the energy range ΔE, the latter being a measure of the curvature of $E(\theta)$:

$$E_{av}^{tm0} = \frac{1}{\pi}\int_0^\pi E_0(\theta)\mathrm{d}\theta \quad (2)$$

$$E_{av}^{tm0} = -\frac{4C}{d\pi}\left[\left(\frac{K\left(\frac{-4\frac{\ell}{d}}{\left(1-\frac{\ell}{d}\right)^2}\right)}{1-\frac{\ell}{d}}\right) + \left(\frac{K\left(\frac{4\frac{\ell}{d}}{\left(1+\frac{\ell}{d}\right)^2}\right)}{1+\frac{\ell}{d}}\right)\right] \quad (3)$$

$$E_{av}^{tm0} \approx -\frac{4C}{d}\left[1+\frac{1}{4}\left(\frac{\ell}{d}\right)^2\right] \quad (\ell \ll d) \quad (4)$$

$$\Delta E^{tm0} = E_0(\theta_{max}) - E_0(\theta_{min}) \quad (5)$$

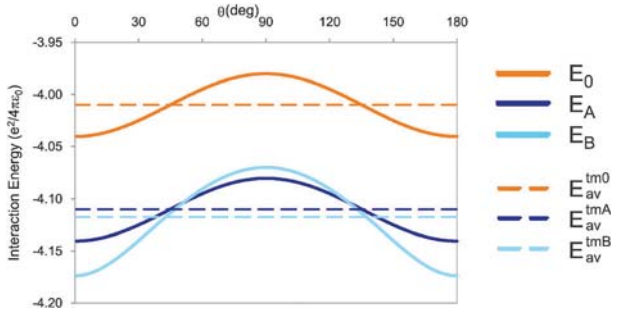

Fig. 2 Full lines: total energy for the three toy models, as a function of the orientation of the nucleus. Dashed lines: average energy. In order to exaggerate and emphasize the differences, the graphs are made with the values $\frac{\varepsilon}{e} = 0.005$, $\frac{\ell}{d} = 0.1$ and $n = 2$.

Table 1 Order of magnitude values of some key quantities for a set of elements: the total electron charge (and nuclear charge) $\pm 2e$ (unit: elementary charge e). The electron–nucleus distance d, taken as the atomic radius from Clementi *et al.*[7] The number of electrons inside the nucleus (ε), taken as the electron charge density at the nuclear center (from Clementi and Roetti[8] and Gálvez and Porras,[9] supplemented by our own *ab initio* calculations) multiplied by the nuclear volume. The distance of the intranuclear electrons from the origin (a, unit: attometer) and the corresponding fractional value $n = \ell/a$, determined by matching eqn (34) to estimated quadrupole anomalies (Table 2). The nuclear radius ℓ, taken from Angeli.[10] The ratio of electrons inside and outside the nucleus (ε/e), and the ratio of nuclear radius and electron–nucleus distance (ℓ/d)

Symbol	Unit	Li	K	Rb	I	Hf	Re	U
$2e$	e	3	19	37	53	72	75	92
d	Å	1.67	2.43	2.65	1.15	2.08	1.88	1.75
ε	10^{-8} e	3.5×10^{-6}	6.5×10^{-3}	0.15	1.1	9.2	13	92
a	am	0.15	0.19	0.25	0.87	0.29	0.32	0.24
n	10^3	13	17.5	17.3	5.5	18.3	16.8	24
ℓ	fm	2.0	3.4	4.3	4.8	5.3	5.4	5.8
ε/e	10^{-9}	1.2×10^{-5}	0.0034	0.041	0.21	1.3	1.7	10
ℓ/d	10^{-5}	1.2	1.4	1.6	4.2	2.5	2.9	3.3

$$\Delta E^{\mathrm{tm0}} = -2C\left(\frac{2}{\sqrt{d^2+\ell^2}} - \frac{1}{d-\ell} - \frac{1}{d+\ell}\right) \tag{6}$$

$$\Delta E^{\mathrm{tm0}} \approx \frac{2C}{d}\left(\frac{\ell}{d}\right)^2 \quad (\ell \ll d). \tag{7}$$

The derivation of E_{av} is elaborated upon in the Appendix. $K(x)$ is the complete elliptic integral of the first kind, a special function that can be found either by tabulations or by mathematical software. $\theta_{\max}$ ($\theta_{\min}$) is the angle for which E_0 reaches its maximal (minimal) value. The approximate expressions (eqn (4) and (7)) are series expansions in the small term ℓ/d, up to the quadratic term. They are valid when $\ell \ll d$, which is a realistic approximation in the case of an atom (see also Table 1). Eqn (4) and (7) clearly express the influence of the shape of the nucleus on the energy: for a point nucleus ($\ell = 0$), the energy E_0 does not depend on θ at all. It adopts the constant value $E_{\mathrm{av}} = -4C/d$, and the curvature ΔE is zero. With a dumb-bell type of nucleus ($\ell > 0$), the average energy becomes more negative than $-4C/d$, and the curvature increases. Both the lowering of the average value and the increase of the curvature depend quadratically on ℓ/d, not linearly.

2.3 Electrons inside the nucleus: tmA

The second toy model that will be discussed, is called tmA (Fig. 1(c)). It is identical to tm0, except for the fact that in addition to the two negative point charges, it has an extra spherical homogeneous charge distribution with total charge $-\varepsilon$ centered at the origin.§ This sphere lies entirely inside the volume covered by the nucleus. The charge $-\varepsilon$ can be thought of as being small with respect to $-e$ ($\varepsilon \ll e$) in order to be more similar to what happens in real atoms, but for the solutions we discuss here this is not necessary. Considering Gauss' law, it is obvious that the electric potential at any point outside the sphere will not depend on whether the charge $-\varepsilon$ is distributed homogeneously over the volume of the sphere, or rather over a two-dimensional spherical shell. The potential will not depend on the radius of the sphere either, and will be the same even if the sphere shrinks to a point charge $-\varepsilon$ at the center of the nucleus. Moreover, due to the spherical symmetry of the problem, the additional electrostatic interaction between the nucleus and this new charge distribution will not depend on the orientation of the nucleus – it leads to a constant shift of the interaction energy when compared to tm0:

$$E_{\mathrm{A}}(\theta) = E_0(\theta) + \underbrace{\frac{-2\varepsilon C}{e\ell}}_{E_{\mathrm{corA}}}. \tag{8}$$

As is seen in Fig. 2, the total energy shifts downwards. This shift (E_{corA}) is the (*total*) *monopole shift* for tmA w.r.t. tm0. The monopole shift depends on the nuclear charge ($+2e$), the size of the nucleus (ℓ) and the amount of electron charge inside the nucleus ($-\varepsilon$). It does not depend on the orientation of the nucleus (θ). Concerning the two quantities that characterize the angular dependence of the energy, we see that the average value of the energy shifts by the same amount, whereas the curvature is unchanged:

$$E_{\mathrm{av}}^{\mathrm{tmA}} = E_{\mathrm{av}}^{\mathrm{tm0}} + E_{\mathrm{corA}} \tag{9}$$

$$\Delta E^{\mathrm{tmA}} = \Delta E^{\mathrm{tm0}}. \tag{10}$$

In a non-relativistic treatment, only s-electrons have a non-vanishing probability at $r = 0$, *i.e.* inside the nucleus. As s-electron orbitals are spherically symmetric, tmA is a valid model for non-relativistic s-electron penetration. Table 1 lists the values of the intranuclear electron charge ε for a few elements – it is extremely small, ranging from 10^{-14} to 10^{-7} elementary charges.

3 Monopole shift physics

3.1 Isotope shift

In atomic spectroscopy, the *isotope shift* refers to the small differences in the position of atomic energy levels for different isotopes ${}^{A_1}X$ and ${}^{A_2}X$ of the same element X (A_1 and A_2 are atomic mass numbers and X can be any element). All such isotopes have the same charge (same number of protons), yet a different mass (different number of neutrons). This explains one part of the effect (the *mass shift*): different masses lead to a (slightly) different position of the center of mass of the atom, and this affects the energy levels in a way that is well-understood.[11] It is the other part of the effect, however, that interests us here: the *field shift*. It is illustrated in Fig. 3 by two versions of tmA: a different number of neutrons leads in general to a different size of the nucleus, expressed by a different mean square radius. Therefore, in Fig. 3, the two toy atoms have a 'nucleus' with a different length 2ℓ for the rigid rod. This difference in ℓ will lead to a different interaction energy in the case without electrons inside the nucleus (tm0, eqn (1)).

§ One can argue that a better analog with reality is obtained if the total electron charge of tm0 would be redistributed in order to yield tmA: charges $-e + \varepsilon/2$ outside the nucleus and a charge $-\varepsilon$ inside, keeping the total electron charge at $2e$. This is correct. However, it makes the resulting equations less simple, and it does not really affect the final results. We will see that for realistic values of ε and ℓ the contribution to the interaction energy from charges outside the nucleus is almost insensitive to ε and ℓ. Therefore, we opt for the simpler toy models with $-2e$ as electron charge outside the nucleus for all of them.

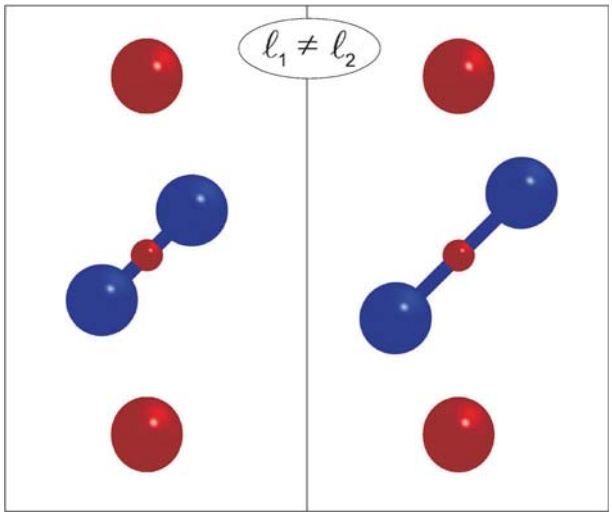

Fig. 3 The isotope shift: two isotopes of the same element with the same electron distribution (including an identical isotropic part inside the nucleus), yet a different nuclear size ($\ell_1 \neq \ell_2$). This will lead to different interaction energies for tmA, and the difference is in the first place due to the electrons inside the nucleus.

However, this is a vanishingly small effect, as can be understood by taking the derivative of $E_{\mathrm{av}}^{\mathrm{tm0}}$ (eqn (3) or (4)) with respect to ℓ:

$$\frac{\mathrm{d}E_{\mathrm{av}}^{\mathrm{tm0}}}{\mathrm{d}\ell} \approx -\frac{2C}{d^3}\ell. \qquad (11)$$

Indeed, in the limit of a nucleus that is much smaller than the size of the electron cloud ($\ell \ll d$, or $\lim_{\ell \to 0}$) – which is the situation that applies to real atoms (Table 1) – this derivative is zero: the average interaction energy of tm0 hardly depends on the size of the nucleus. This changes when there are electrons inside the nucleus (tmA, eqn (9)). The derivative of the average energy for tmA with respect to ℓ is:

$$\frac{\mathrm{d}E_{\mathrm{av}}^{\mathrm{tmA}}}{\mathrm{d}\ell} = \frac{\mathrm{d}E_{\mathrm{av}}^{\mathrm{tm0}}}{\mathrm{d}\ell} + \frac{2\varepsilon C}{e}\frac{1}{\ell^2}. \qquad (12)$$

Even though there is a small factor ε/e in the second term ($\varepsilon \ll e$, see Table 1), for sufficiently small values of ℓ this term becomes arbitrarily large. Hence, when there are electrons inside the nucleus, the nuclear size has a significant impact on the average interaction energy of tmA. This is the field shift contribution to the isotope shift. It is experimentally observable by measuring the energy that is required for total ionization of a free atom for each isotope.

Toy models tm0 and tmA show the physics behind the field shift. The key issue is the factor $1/r$ in the electrostatic potential. For electrons outside the nucleus, r has the order of magnitude of 1 Å ($d \pm \ell$ in tm0): $1/r$ is small and flat. For electrons inside the nucleus, r is a few femtometers (the order of magnitude of ℓ): $1/r$ is large and steep. Variations in ℓ between different isotopes are of the order of magnitude of hundreds of femtometers. This leads to variations in $1/r$ that are negligible for electrons outside the nucleus, but significant for electrons inside the nucleus.

3.2 Isomer shift

Another effect that originates from the monopole shift, is the *isomer shift* in Mössbauer spectroscopy. There is an extensive body of literature about this property, and about how it can be used to obtain local information about chemical bonds in solids.[12–14] For our present purpose, the following concise definition should be sufficient: the isomer shift gives the energy difference between a nuclear transition observed with an isotope ^{A}X embedded in one solid (called 'the source'; s) and the same transition observed with the same isotope embedded in another solid (called 'the absorber'; a). The shape of the electron cloud of atom X, which is characterized by d and ε, characterizes the chemical bonding of these atoms in their respective solids. These properties are different for the source and the absorber (d_{s} and ε_{s} *vs.* d_{a} and ε_{a}). Furthermore, for both source and absorber, two nuclear states will be involved: the ground state (g) and the excited nuclear state (e) (*i.e.* a structural isomer) of that particular isotope ^{A}X. In both states, the nucleus has the same number of protons and neutrons, yet these are differently configured. Therefore, the nuclear size (characterized by ℓ) is different for both states (ℓ_{g} *vs.* ℓ_{e}). The nuclear property ℓ itself does not affect the electron properties d and ε.

All together, this gives 4 different situations, which are the ones that are shown in Fig. 4: the excited nuclear state for the

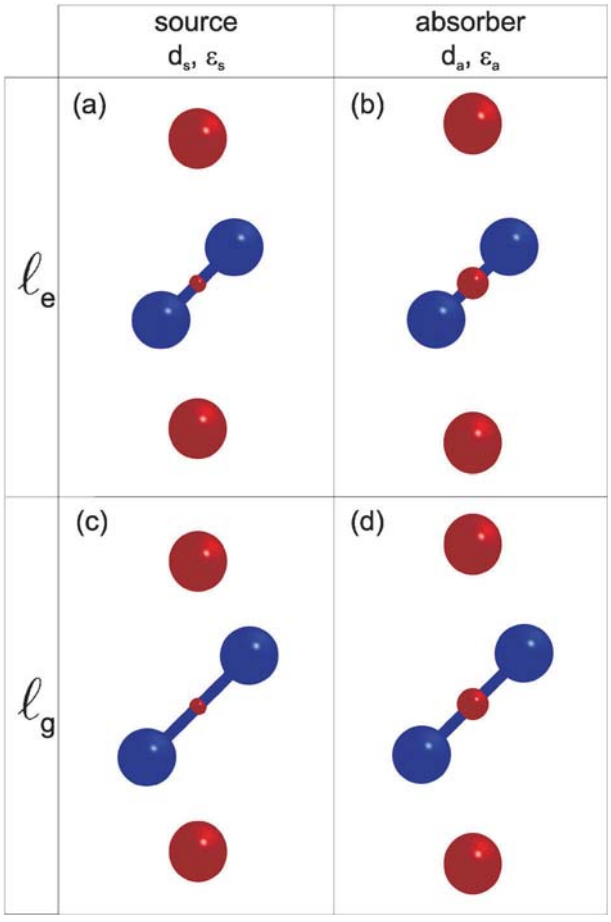

Fig. 4 The four different situations for tmA that appear in our toy model for the isomer shift (see text).

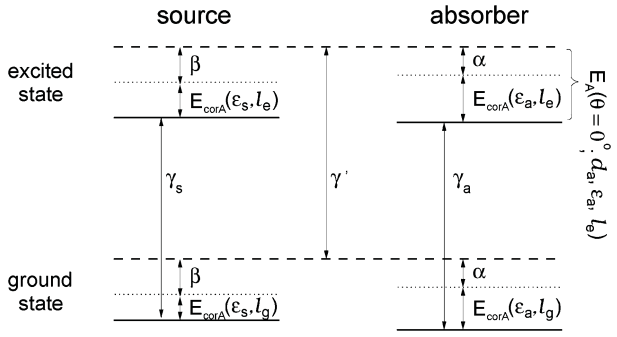

Fig. 5 Energy levels involved in the isomer shift (see text).

atom embedded in the source (Fig. 4(a): ℓ_e, d_s, ε_s), the excited nuclear state for the atom embedded in the absorber (Fig. 4(b): ℓ_e, d_a, ε_a), the nuclear ground state for the atom embedded in the source (Fig. 4(c): ℓ_g, d_s, ε_s), and the nuclear ground state for the atom embedded in the absorber (Fig. 4(d): ℓ_g, d_a, ε_a).

Fig. 5 summarizes the key features of the isomer shift. We start discussing this picture at the upper right corner, which represents the interaction energy of the toy model for the absorber solid and the excited nuclear state (*cf.* Fig. 4(b)). The dashed line represents the zero level for the interaction energy, *i.e.* the excited toy nucleus and the electron charges are at an infinite distance from each other. The solid line represents the lowest interaction energy level for this excited state toy nucleus model ($\theta = 0°$). The difference between the dashed and full lines is $E_A(\theta = 0°; d_a, \varepsilon_a, \ell_e)$ (eqn (8)). According to eqn (8), this energy difference can be separated into two terms: the first term $E_0(\theta = 0°; d_a, \ell_e)$ (indicated by α in Fig. 4 and identical to eqn (1)), and the second term, $E_{corA}(\varepsilon_a, \ell_e)$. It requires an energy release of typically several keV to MeV to transform the nucleus from its excited state (ℓ_e) to its ground state (ℓ_g). Therefore, the zero level for the interaction energy between the electron cloud in the absorber solid and the nucleus in its ground state (*i.e.* the dashed line in bottom-right of Fig. 5), lies on an absolute energy scale much below the zero level for the previous situation. Hence, the picture is not on the scale. The energy difference between these two zero levels (*i.e.* between the two dashed lines) – which we call γ' – is the energy it takes to transform the nucleus from the ground state to the excited state. The lowest interaction energy level for this ground state toy nucleus model is given by eqn (8) with $\theta = 0°$ and $d = d_a$, $\varepsilon = \varepsilon_a$ and $\ell = \ell_g$. According to eqn (8), the first term of this energy is $E_0(\theta = 0°; d_a, \ell_g)$ (eqn (1)). However, as we saw in Section 3.1, this is for realistic situations nearly identical to $E_0(\theta = 0°; d_a, \ell_e)$. Therefore, we indicate it by the same value α. The second part of the interaction energy is given by the second term from eqn (8), which we call here $E_{corA}(\varepsilon_a, \ell_g)$. We saw in Section 3.1 that this term does depend significantly on the value of ℓ. Therefore, we arrive at the following conclusion: the effective energy γ_a required to transform the entire toy model for the absorber solid from its lowest interaction energy level with the ground state toy nucleus to its lowest interaction energy level with the excited state toy nucleus, is not given exclusively by the energy γ' (the energy to transform an isolated nucleus), but has an additional part that is determined by the nuclear size and the electron charge inside the nucleus:

$$\gamma_a = \gamma' - E_A(\theta = 0°; d_a, \varepsilon_a, \ell_e) + E_A(\theta = 0°; d_a, \varepsilon_a, \ell_g) \approx \gamma' - \frac{2C\varepsilon_a}{e}\left(\frac{1}{\ell_e} - \frac{1}{\ell_g}\right). \quad (13)$$

Exactly the same reasoning can be made for the source material (left sides of Fig. 4 and 5), resulting in:

$$\gamma_s = \gamma' - E_A(\theta = 0°; d_s, \varepsilon_s, \ell_e) + E_A(\theta = 0°; d_s, \varepsilon_s, \ell_g) \approx \gamma' - \frac{2C\varepsilon_s}{e}\left(\frac{1}{\ell_e} - \frac{1}{\ell_g}\right). \quad (14)$$

The correction due to E_A to the bare nuclear energy difference γ' is 10 orders of magnitude smaller than γ' itself, and is too small to be experimentally observable. However, Mössbauer spectroscopy is capable of measuring the *difference* between the effective transition energies:

$$\Delta\gamma = \gamma_a - \gamma_s \quad (15)$$

$$\Delta\gamma \approx \frac{-2C}{e}(\varepsilon_a - \varepsilon_s)\left(\frac{1}{\ell_e} - \frac{1}{\ell_g}\right). \quad (16)$$

The quantity $\Delta\gamma$ is the *isomer shift*, and its toy model expression eqn (16) is extremely similar to the isomer shift formula that is very well known in the Mössbauer community.¶ The isomer shift is entirely determined by the size difference of the nucleus in its ground and excited states (a nuclear property), and the difference between the electron charge inside the nucleus in source and absorber material (a solid state property). By the latter, the isomer shift is sensitive to very local details of the chemical bonding, and can be used for instance as a fingerprint for the position of an atom in a solid.

4 Toy model: tmB

We now move on to a new kind of toy model, that is essentially different from tm0 or tmA, and that therefore will show qualitatively different observable effects. This toy model – which we call tmB from here on – is shown in Fig. 1(d). The electron charge outside the nucleus is identical to tm0 and tmA. Inside the nucleus, tmB has two point charges $-\varepsilon/2$ that form a fixed dumb-bell on the Z-axis, *i.e.* aligned with the dumb-bell formed by the two external charges $-e$. Each of these two point charges lies at a distance a from the origin. It will be convenient later to express a as a fraction of the nuclear radius: $a = \ell/n$, with n being a real number that is strictly larger than 1 ($n > 1$). Both tmA and tmB have the same total charge $-\varepsilon$ inside the nucleus. The crucial difference between them is that this charge has spherical symmetry for tmA, but not for tmB. As a consequence, the additional interaction energy due to the electron charge inside the nucleus does

¶ The common expression for the isomer shift contains charge densities [C/m^3] multiplied by nuclear mean square radii [m^2]. This leads to the same dimensions [C/m] as in eqn (16), where charges [C] are divided by nuclear radii [m].

depend on the orientation of the nucleus (compare eqn (17) with eqn (8) for tmA):

$$E_{\mathrm{B}}(\theta) = E_0(\theta) + E_{\mathrm{corB}}(\theta) \tag{17}$$

with (for $\ell > a$)

$$E_{\mathrm{corB}}(\theta) = -\frac{\varepsilon C}{e}\left(\frac{1}{\sqrt{\ell^2\sin^2\theta + (\ell\cos\theta - a)^2}} + \frac{1}{\sqrt{\ell^2\sin^2\theta + (\ell\cos\theta + a)^2}}\right). \tag{18}$$

In the limiting case $a \to 0$ (or $n \to \infty$), tmB becomes equal to tmA. Indeed: for this limit, eqn (17) becomes equal to eqn (8). Graphically, eqn (17) translates into an interaction energy $E_{\mathrm{B}}(\theta)$ that is not only shifted downwards with respect to $E_0(\theta)$ (as $E_{\mathrm{A}}(\theta)$ was), but which has additionally also a different curvature (Fig. 2). This can also be seen in the average energy and the energy range for tmB (using $a = \ell/n$, with $n > 1$):

$$E_{\mathrm{av}}^{\mathrm{tmB}} = E_{\mathrm{av}}^{\mathrm{tm0}} - \underbrace{\frac{2\varepsilon C}{e\ell}\frac{n}{\pi}\left[\frac{K\left(\frac{-4n}{(n-1)^2}\right)}{n-1} + \frac{K\left(\frac{4n}{(n+1)^2}\right)}{n+1}\right]}_{f(n)} \tag{19}$$

$$E_{\mathrm{av}}^{\mathrm{tmB}} = E_{\mathrm{av}}^{\mathrm{tm0}} + f(n)E_{\mathrm{corA}} \tag{20}$$

$$\Delta E^{\mathrm{tmB}} = \Delta E^{\mathrm{tm0}} - \frac{2\varepsilon C}{e\ell}\underbrace{\left(\frac{n}{\sqrt{1+n^2}} - \frac{n^2}{n^2-1}\right)}_{p(n)} \tag{21}$$

$$\Delta E^{\mathrm{tmB}} \approx \Delta E^{\mathrm{tm0}} + \frac{3\varepsilon C}{e\ell n^2} \tag{22}$$

In eqn (20), the average energy for tmB is written as a function of the average energy for tmA. The difference between both is expressed by the function $f(n)$:

$$f(n) = \frac{n}{\pi}\left[\frac{K\left(\frac{-4n}{(n-1)^2}\right)}{n-1} + \frac{K\left(\frac{4n}{(n+1)^2}\right)}{n+1}\right] \tag{23}$$

$$f(n) \approx 1 + \frac{1}{4n^2} \quad (n \gg 1). \tag{24}$$

In the limit $n \to \infty$, tmB evolves to tmA. This is consistent with the fact that $\lim_{n\to\infty} f(n) = 1$ (Fig. 6). Because $f(n) > 1$, the average energy for tmB is always more negative than the average energy for tmA, regardless of the value of n. Moreover, unless n is only marginally larger than 1, the value of $f(n)$ is close to 1: the average energy for tmB is only slightly below the average energy for tmA (see also Fig. 2). This means that it is in the first place the *amount* of electron charge inside the nucleus that determines the change in average energy (monopole shift). The *anisotropy* of the electron charge inside the nucleus has hardly an impact on the average energy.

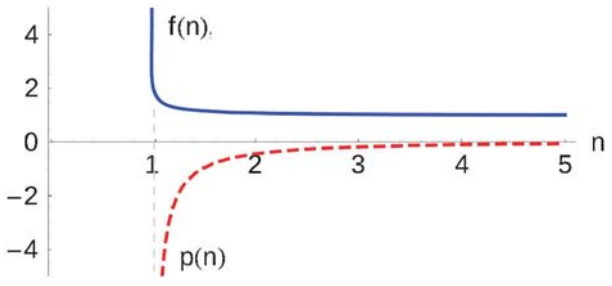

Fig. 6 The functions $p(n)$ (eqn (21)) and $f(n)$ (eqn (23)).

The effect of this anisotropy manifests itself elsewhere. For any allowed value of n, ΔE^{tmB} is larger than $\Delta E^{\mathrm{tm0}} = \Delta E^{\mathrm{tmA}}$. This is a consequence of $p(n)$ being always negative (Fig. 6). The increase is maximal for n being barely larger than 1, and tends to zero for large values of n, when tmB becomes equal to tmA. The former case ($n \gtrsim 1$) corresponds to a highly anisotropic electron charge distribution inside the nuclear volume. The latter case ($n \to \infty$, or tmB $\to$ tmA) corresponds to an almost spherical electron charge distribution inside the nuclear volume. The increase in the energy range and the corresponding increase in the curvature are therefore proportional to the degree of anisotropy of the electron charge distribution inside the nucleus (large curvature change = large anisotropy = small n ($n \approx 1$)):

$$\underbrace{\Delta E^{\mathrm{tmB}} - \Delta E^{\mathrm{tm0}}}_{\Delta E_{\mathrm{cor}}^{\mathrm{tmB}}} \approx \frac{3\varepsilon C}{e}\frac{1}{\ell n^2} \tag{25}$$

$$\underbrace{\Delta E^{\mathrm{tmB}} - \Delta E^{\mathrm{tm0}}}_{\Delta E_{\mathrm{cor}}^{\mathrm{tmB}}} \approx \frac{3\varepsilon C}{e}\frac{1}{an^3}. \tag{26}$$

This change in curvature represents the *(total) quadrupole shift* for tmB w.r.t. tm0 or tmA, which depends on the nuclear charge ($+2e$), the size of the nucleus (ℓ), the amount of electron charge inside the nucleus ($-\varepsilon$) and the deviation from spherical symmetry of this electron charge (expressed by n and/or a).

Whereas a spherically symmetric charge distribution inside the nucleus is realized in Nature by s-electrons, a non-spherical charge distribution is realized by relativistic $p_{1/2}$-electrons (non-relativistic p-electrons do not enter the nucleus). Therefore, tmB is a valid model for relativistic aspects of electron penetration into the nucleus. The survey of realistic values in Table 1 shows that the anisotropy of the intranuclear electron distribution is extremely small: the separation between the two $-\varepsilon/2$ point charges is measured in attometer, which is 3 to 4 orders of magnitude smaller than the dimensions of the nucleus (therefore $n \gg 1$). This allows making a series expansion in the small factor $1/n$, which transforms eqn (21) into the simpler eqn (22).

5 Quadrupole shift physics

5.1 Regular quadrupole shift

Now, we apply again the arguments that were developed in Section 3.1 for the average interaction energy E_{av}, but this time for the curvature ΔE. Two isotopes of the same element, will usually have a different nuclear radius ℓ. We have seen in Section 3.1 that this affects the average energy significantly only if there is an electron charge inside the nuclear volume (tmA).

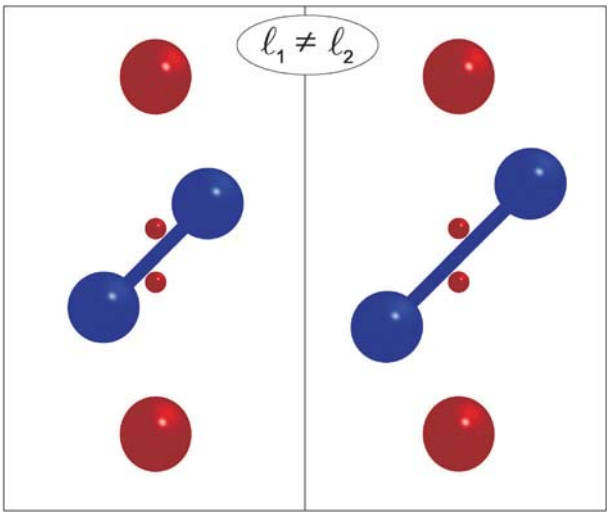

Fig. 7 The quadrupole shift: two isotopes of the same element with the same electron distribution (including an identical anisotropic part inside the nucleus), yet a different nuclear shape ($\ell_1 \neq \ell_2$). This will lead to different interaction energies for tmB, and the difference is in the first place due to the electrons inside the nucleus.

How does the energy curvature ΔE depend on ℓ? For tm0, the derivative of the curvature with respect to ℓ is:

$$\frac{\mathrm{d}\Delta E^{\mathrm{tm0}}}{\mathrm{d}\ell} = \frac{4C}{d^3}\ell. \tag{27}$$

According to eqn (10), exactly the same expression holds for tmA. In the limit $\ell \ll d$ or $\ell \to 0$, this expression tends to zero: the curvature depends negligibly on the nuclear size, regardless of whether there are spherically symmetric electron charges inside the nucleus (tmA) or no electrons at all inside the nucleus (tm0). This becomes different for tmB, with anisotropic electron charges inside the nucleus (Fig. 7):

$$\frac{\mathrm{d}\Delta E^{\mathrm{tmB}}}{\mathrm{d}\ell} = \frac{\mathrm{d}\Delta E^{\mathrm{tm0}}}{\mathrm{d}\ell} + \frac{2\varepsilon C}{e}\left(\frac{n}{\sqrt{1+n^2}} - \frac{n^2}{n^2-1}\right)\frac{1}{\ell^2}. \tag{28}$$

In the same limit, $\lim_{\ell \to 0}$, this expression tends to infinity: with anisotropic electron charges inside the nucleus, the curvature becomes significantly more sensitive to the nuclear size.

For realistic atoms, the curvature due to electrons outside the nucleus (ΔE^{tm0}) is several orders of magnitude larger than the curvature due to electrons inside the nucleus ($\Delta E^{\mathrm{tmB}}_{\mathrm{cor}}$) (see Koch *et al.*,[6] and also eqn (21) with values from Table 1). Curvatures ΔE are experimentally accessible as the so-called *quadrupole coupling constant* ν_{Q}:

$$\nu_{\mathrm{Q}} = \frac{eQV_{zz}}{h} \tag{29}$$

where h is Planck's constant, Q is the nuclear property (the *nuclear quadrupole moment*, which expresses the deviation from spherical symmetry of the nucleus), and V_{zz} is the electron property (the *electric-field gradient*, which expresses the deviation from spherical symmetry of the electron distribution at the position of the nucleus). For our toy models, Q is proportional to ℓ^2, and V_{zz} is proportional to $1/d^3$. The electron property V_{zz} can be determined by first-principles electronic structure calculations. Knowing V_{zz} (calculated) and ν_Q (measured), Q can be determined from eqn (29). Such a procedure is routinely used to determine the nuclear quadrupole moment Q of isotopes (see Koch *et al.*[6] and references therein). In toy model language, it means that the nuclear property ℓ^2 can be determined from eqn (21) if the electron quantities d, ε and n and the experimental quantity ΔE are known. The precision by which the electron properties can be calculated, limits the precision by which the nuclear property (Q) can be determined. As a matter of fact, the resulting uncertainty in the nuclear property is that large that it is useless to take the small correction $\Delta E^{\mathrm{tmB}}_{\mathrm{cor}}$ (or ε and n) into account. Experimentally observed ΔE values can be explained within their error bar by the ΔE^{tm0} term alone. This is different from the case of the isotope shift, where the correction term E_{corA} in eqn (9) is significantly larger than the experimental error bar.

From this point of view, the quadrupole shift $\Delta E^{\mathrm{tmB}}_{\mathrm{cor}}$ is *de facto* not experimentally observable. As we have pointed out in a recent paper,[6] however, several 'curvature' experiments can be combined in such a way that a quantity is obtained that is sensitive to the quadrupole shift: this is the *quadrupole anomaly*, which will be discussed in the next section.

5.2 Quadrupole anomaly

Albeit the nuclear quadrupole moment Q can often be determined with limited precision only, the ratio Q_1/Q_2 between the quadrupole moments of two isotopes of the same element can be known with much higher accuracy. The reason for this can be understood by inspecting tm0. Imagine a curvature $\Delta E^{\mathrm{tm0}}_1$ being measured for isotope 1 (characterized by ℓ_1), in a given electron environment characterized by $d = d_1$. The same is done for another isotope of the same element (ℓ_2), embedded in the same electron environment ($d = d_2 = d_1$). According to eqn (7), the ratio of curvatures – which is itself an experimentally accessible number – is given by:

$$\frac{\Delta E^{\mathrm{tm0}}_1}{\Delta E^{\mathrm{tm0}}_2} \approx \underbrace{\left(\frac{d_2}{d_1}\right)^3}_{=1}\left(\frac{\ell_1}{\ell_2}\right)^2. \tag{30}$$

Without electrons inside the nucleus, the ratio of experimentally known curvatures depends only on the ratio of nuclear radii (translated into real atoms, it means that the ratio of quadrupole coupling constants depends on the ratio of nuclear quadrupole moments – see eqn (44) in ref. 6). According to eqn (10), the same holds for a spherically symmetric electron distribution inside the nucleus. As curvatures (quadrupole coupling constants) can be measured with high precision, ratios of curvatures – and therefore also ratios of nuclear properties (quadrupole moments) – can be known with high precision too.

This becomes different once we allow non-isotropic electron charges inside the nucleus (tmB). According to eqn (21), the ratio between the curvatures for two different isotopes in the same electron environment is ('environment A', Fig. 8, left):

$$\left.\frac{\Delta E^{\mathrm{tmB}}_1}{\Delta E^{\mathrm{tmB}}_2}\right|_{\mathrm{envA}} \approx \left(\frac{\ell_1}{\ell_2}\right)^2 \left(\frac{1 - \frac{\varepsilon_{\mathrm{a}}}{e}\left(\frac{d_{\mathrm{a}}}{\ell_1}\right)^3 p(n_{\mathrm{a}})}{1 - \frac{\varepsilon_{\mathrm{a}}}{e}\left(\frac{d_{\mathrm{a}}}{\ell_2}\right)^3 p(n_{\mathrm{a}})}\right) \tag{31}$$

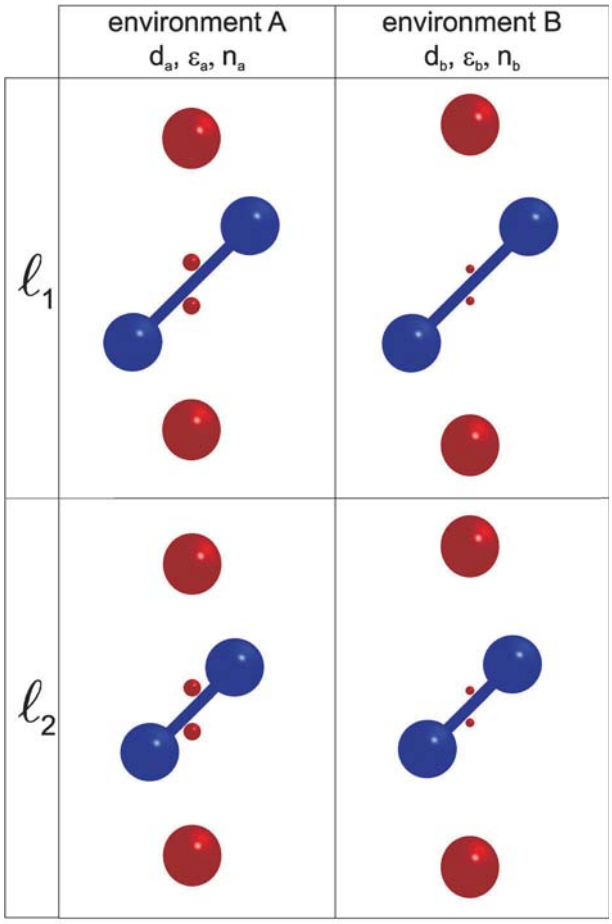

Fig. 8 The four different situations for tmB that appear in our toy model for the quadrupole anomaly (see text).

$$\left.\frac{\Delta E_1^{\mathrm{tmB}}}{\Delta E_2^{\mathrm{tmB}}}\right|_{\mathrm{envA}} \approx \left(\frac{\ell_1}{\ell_2}\right)^2 \left[1 + \frac{\varepsilon_a d_a^3}{e} p(n_a)\left(\frac{1}{\ell_2^3} - \frac{1}{\ell_1^3}\right)\right] \qquad (32)$$

($d_a = d_1 = d_2$, $\varepsilon_a = \varepsilon_1 = \varepsilon_2$, $n_a = n_1 = n_2$, $\ell_1 \neq \ell_2$). In order to obtain eqn (31), the approximate expression eqn (7) was used. Eqn (32) is obtained after a further approximation (power series expansion), which is valid when $\frac{\varepsilon}{e}\frac{d^3}{\ell^3}\, p(n) \ll 1$, which is true in real cases (easily verified from Table 1). The ratio of curvatures does *not* depend on the simple nuclear ratio ℓ_1/ℓ_2 any longer. Only if the electron charge inside the nucleus becomes isotropic ($n \to \infty$ or tmB $\to$ tmA), or if the electron charge inside the nucleus vanishes ($\varepsilon \to 0$ or tmB $\to$ tm0), the simple dependence is restored. Albeit the deviation from unity in eqn (31) or (32) is small, it is large enough to affect curvature ratio experiments (= quadrupole coupling experiments) outside the experimental error bar. Nevertheless, although the measured ratios are affected by the presence of anisotropic charges inside the nucleus, eqn (31) or (32) does not lead to useful interpretations yet: no subset of quantities from (ℓ_1, ℓ_2, n, ε, d) is known *a priori* with a sufficient precision to extract more precise values for any of the remaining quantities of the set. An observable effect eventually arises when the curvature ratio experiment is repeated for the same two isotopes being embedded in a second, different electron environment ('environment *B*', Fig. 7, right):

$$\delta = \left.\frac{\Delta E_1^{\mathrm{tmB}}}{\Delta E_2^{\mathrm{tmB}}}\right|_{\mathrm{envA}} - \left.\frac{\Delta E_1^{\mathrm{tmB}}}{\Delta E_2^{\mathrm{tmB}}}\right|_{\mathrm{envB}} \qquad (33)$$

$$\delta \approx \left(\frac{\ell_1}{\ell_2}\right)^2 \left(\frac{\varepsilon_a}{e} d_a^3 p(n_a) - \frac{\varepsilon_b}{e} d_b^3 p(n_b)\right)\left(\frac{1}{\ell_2^3} - \frac{1}{\ell_1^3}\right). \qquad (34)$$

The quantity δ that is defined in this way, is the *quadrupole anomaly*.‖ As it is obtained from four ΔE values, it is directly available from experiment. The quadrupole anomaly becomes zero when there are no electrons inside the nucleus (ε_a, $\varepsilon_b \to 0$), or when the electron distribution inside the nucleus is spherically symmetric (n_a, $n_b \to \infty$). Measuring the quadrupole anomaly is therefore a way to get experimental information on the anisotropy of the electron distribution inside the nucleus.

6 Experimental status

Whereas the isotope shift and the Mössbauer isomer shift are properties that are routinely measured in atomic spectroscopy and Mössbauer spectroscopy, the quadrupole anomaly is a 'new' property. We have recently suggested[6] a way to measure it by high-precision molecular spectroscopy – this method is outlined in Section 5.2 using the toy models. The very recent experimental literature shows that the first observation of a quadrupole anomaly might have become reality.

Table 2 lists several experimental realizations of the set of 4 situations that were described in Fig. 8 and in Section 5.2: 2 different isotopes of the same element, measured in 2 different diatomic molecules, leading to 4 measurements. The property that is measured is the quadrupole coupling constant ν_Q (eqn (29)). The quadrupole coupling constant corresponds to the curvature ΔE for the toy models. For either of both molecules, the ratio of the quadrupole coupling constants for both isotopes is listed in Table 2. The difference between these ratios is the experimental quadrupole anomaly δ_{exp} (eqn (33)). An order of magnitude estimate δ_{est} for the quadrupole anomaly, based on *ab initio* calculations, is listed as well.[6] The question at stake is: have experiments convincingly shown that δ can be different from zero?

Among the six quartets that are listed in Table 2, two lead to a δ_{exp} that is different from zero beyond the error bar: K in KF and KI, and Rb in RbF and RbI. In the former case, the observed value of δ is three orders of magnitude larger than expected. This makes it unlikely that this is due to a quadrupole anomaly. Either there is a problem with the interpretation of the experimental results, or other effects

‖ In Koch *et al.*,[6] we defined the quadrupole anomaly δ in analogy to the hyperfine anomaly Δ (Bohr–Weisskopf effect): as the deviation from unity of a particular quadrupole coupling constant ratio (eqn 44 in Koch *et al.*[6] or eqn (32) in the present work). However, in contrast to the hyperfine anomaly, this type of quadrupole anomaly cannot be experimentally determined with meaningful accuracy. Therefore, from the present paper onwards, we define the quadrupole anomaly δ as in eqn (33): as the *difference* between two particular quadrupole coupling constant ratios. This is an experimentally observable quantity, and it is therefore more meaningful to use the symbol δ and the word 'quadrupole anomaly' for this concept.

Table 2 Ratios of experimental quadrupole coupling constants (third column) for two different isotopes ("1" and "2") in two different molecules, collected from the literature (updated from ref. 6). Experimental values for the quadrupole anomaly δ_{exp} are derived from these using eqn (33). An estimate for the quadrupole anomaly based on *ab initio* calculations[6] is given as well

Molecules	Isotopes	$\Delta E_1^{tmB}/\Delta E_2^{tmB}$	$\lvert\delta_{exp}\rvert$	$\lvert\delta_{est}\rvert$	Ref.
$^{6}Li^{19}F$, $^{7}Li^{19}F$	$^{6}Li/^{7}Li$	0.020161 ± 0.000013	0.00012(15)	6×10^{-10}	15
$^{6}Li^{127}I$, $^{7}Li^{127}I$	$^{6}Li/^{7}Li$	0.02028 ± 0.00014			16
$^{41}K^{19}F$, $^{39}K^{19}F$	$^{41}K/^{39}K$	1.217699 ± 0.000055	0.000206(6)	1×10^{-7}	17
$^{41}K^{127}I$, $^{39}K^{127}I$	$^{41}K/^{39}K$	1.2174935 ± 0.0000099			18
$^{87}Rb^{19}F$, $^{85}Rb^{19}F$	$^{87}Rb/^{85}Rb$	0.4838301 ± 0.0000018	0.000007(24)	1×10^{-6}	19
$^{87}Rb^{35}Cl$, $^{85}Rb^{35}Cl$	$^{87}Rb/^{85}Rb$	0.483837 ± 0.000022			20
$^{87}Rb^{19}F$, $^{85}Rb^{19}F$	$^{87}Rb/^{85}Rb$	0.4838301 ± 0.0000018	0.0000039(30)	1×10^{-6}	19
$^{87}Rb^{127}I$, $^{85}Rb^{127}I$	$^{87}Rb/^{85}Rb$	0.4838262 ± 0.0000012			21
$^{179}Hf^{16}O$, $^{177}Hf^{16}O$	$^{179}Hf/^{177}Hf$	1.13004 ± 0.00001	0.00000(2)	7×10^{-6}	22
$^{179}Hf^{32}S$, $^{177}Hf^{32}S$	$^{179}Hf/^{177}Hf$	1.13004 ± 0.00001			23
$H^{187}Re(CO)_5$, $H^{185}Re(CO)_5$	$^{187}Re/^{185}Re$	0.94636 ± 0.00005	0.000035(55)	7×10^{-6}	24, 25
$CH_3{}^{187}ReO_3$, $CH_3{}^{185}ReO_3$	$^{187}Re/^{185}Re$	0.946325 ± 0.000005			26

manifest themselves (see Koch *et al.*[6]). In the case of Rb in RbF and RbI, the observed difference is in the 6th digit, which is consistent with the estimated order of magnitude. Thanks to very recent high-precision molecular beam electric resonance experiments on RbI,[21] the error bar on $|\delta_{exp}|$ is smaller than $|\delta_{exp}|$ itself, yet only marginally. It is premature to consider this as a proof for the presence of a quadrupole anomaly, yet the search looks promising: if a similar accuracy could be reached for Hf or Re, where the effect is expected to be almost an order of magnitude larger, a more convincing proof could be established. At the theoretical side, it would be worthwhile to predict more precise values for the expected quadrupole anomaly in these molecular quartets, using quantum chemical methods.

As discussed in the appendix of ref. 6, other small quadrupole-like interactions can be present as well, the most important one being the pseudo quadrupole interaction.[1,27] Their presence hinders the unique assignment of non-zero δ values to a quadrupole anomaly. Obtaining precise quantum chemical predictions for these contributions in the cases listed in Table 2 is therefore a worthwhile task as well.

7 Conclusions

The presence of a spherically symmetric electron charge distribution inside the nucleus affects the average value of the interaction energy between nucleus and electrons. This leads to the monopole shift, which can be experimentally observed (isotope shift, isomer shift). We demonstrated in this paper how the monopole shift is present in a very simple classical toy model (tmA), and we used this toy model to build classical analogs for the isotope shift (Fig. 3) and the isomer shift (Fig. 4).

If the distribution of electrons inside the nucleus is *not* spherically symmetric, another and much smaller effect appears: the quadrupole shift. We demonstrated how the quadrupole shift is present in yet another simple toy model (tmB). We used this toy model to illustrate how a combination of 4 well-chosen high-precision molecular spectroscopy experiments can detect the presence of a quadrupole shift *via* the quadrupole anomaly (Fig. 7). Detecting a quadrupole anomaly is at the limit of the currently achievable experimental precision. A survey of the recent experimental literature suggests that an unambiguous demonstration of the existence of the quadrupole anomaly is within reach.

The use of simple, classical toy models displays the physics behind the monopole shift and the quadrupole shift in a most clear way, not troubled by the technical complexity of a relativistic quantum multipole expansion for real molecules. Only Coulomb's law and straightforward calculus are required. It is our hope that the present derivation will contribute to a more wide-spread understanding of, in particular, the quadrupole shift and quadrupole anomaly. Table 1 – which can be easily extended and/or interpolated for other elements – can be used to obtain a quick estimate for the size of these effects in specific situation. Armed with this insight, experimental molecular spectroscopy and quantum chemistry can move on towards a better understanding of these extremely small effects in molecular spectra.

Appendix A: Calculation of E_{av}

Although the average of a function as given by eqn (2) is a simple concept, the actual evaluation of the integral can sometimes be involved. Indeed, this is the only place in this paper where we cannot meet the promise of using elementary calculus only. The indefinite integral in eqn (2) (*i.e.* without the integration limits), with E_0 given by eqn (1), can be found by commonly available symbolic algebra software (Mathematica, Maple, ...). The result contains a special function: the *incomplete elliptic integral of the first kind*, $F(\frac{\alpha}{2}|z)$. In order to find the definite integral given by eqn (2), this function F has to be evaluated for the integration limits $\alpha = 0$ and $\alpha = \pi$ as arguments. It is a property of this special function that it is zero whenever $\alpha = 0$, so one half of the terms drop out. Furthermore, for the specific value $\alpha = \pi$, the following identity holds: $F(\frac{\pi}{2}|z) = K(z)$. Here, $K(z)$ is the *complete elliptic integral of the first kind*, another special function for which numerical values are tabulated or can be found by mathematical software. Its formal definition is:

$$K(z) = \int_0^{\frac{\pi}{2}} \frac{1}{\sqrt{1 - z\sin^2(t)}} \mathrm{d}t \qquad (35)$$

(beware of alternative definitions with $k^2 = z$: $K(k) \neq K(z)$, as the former is symmetric in $\pm k$ and the latter is not).

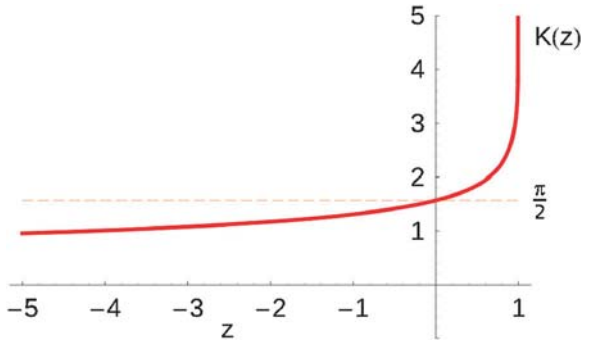

Fig. 9 Values of the complete elliptic integral of the first kind on an interval on the real axis.

The argument z can be complex, but we will need only real arguments. Therefore, also $K(z)$ will be real only. The function $K(z)$ is plotted for the relevant range $z \in [-5, +1]$ in Fig. 9. This leads to the expressions in eqn (3) and (19). The function $K(z)$ can be expanded in a series for $z \approx 0$:

$$K(z) = \frac{\pi}{2}\left(1 + \left(\frac{1}{2}\right)^2 z + \left(\frac{1\times 3}{2\times 4}\right)^2 z^2 + \ldots\right). \qquad (36)$$

Inserting this series in eqn (3), subsequently making an expansion of all factors $(1+\frac{\ell}{d})^n$, and retaining only terms up to second order in ℓ/d, lead to the approximate expression eqn (4). Exactly the same procedure can be used to obtain eqn (24) from eqn (23), as after substituting n by $1/x$ one sees that eqn (23) has the same structure as eqn (3).

Acknowledgements

The authors thank Jens-Uwe Grabow (Gottfried-Wilhelm-Leibniz-Universität, Hannover), Yann Garcia (Université Catholique de Louvain) and Thérèse Huet (Université Lille I) for their critical reading of this manuscript, and Kira Rose for her insight into the toy aspects of this problem. K.R. acknowledges financial support from the Federal Republic of Germany by the *Elternzeit* program. S.C. acknowledges financial support from OCAS NV by an OCAS-endowed chair at Ghent University.

References

1 P. Pyykkö and J. Linderberg, *Chem. Phys. Lett.*, 1970, **5**, 34.
2 J. Thyssen, P. Schwerdtfeger, M. Bender, W. Nazarewicz and P. B. Semmes, *Phys. Rev. A*, 2001, **63**, 022505.
3 G. Karl and V. A. Novikov, *Phys. Rev. C: Nucl. Phys.*, 2006, **74**, 024001.
4 G. Karl and V. A. Novikov, *Phys. Rev. C: Nucl. Phys.*, 2008, **77**, 039901.
5 C. G. Gray, G. Karl and V. A. Novikov, *Am. J. Phys.*, 2009, **77**, 807.
6 K. Koch, K. Koepernik, D. V. Neck, H. Rosner and S. Cottenier, *Phys. Rev. A*, 2010, **81**, 032507.
7 E. Clementi, D. L. Raimondi and W. P. Reinhardt, *J. Chem. Phys.*, 1963, **38**, 2686.
8 E. Clementi and C. Roetti, *At. Data Nucl. Data Tables*, 1974, **14**, 177.
9 F. Gálvez and I. Porras, *Phys. Rev. A*, 1991, **44**, 144.
10 I. Angeli, *At. Data Nucl. Data Tables*, 2004, **87**, 185.
11 W. H. King, *Isotope Shifts in Atomic Spectra*, Plenum Pub. Corp., New York, 1984.
12 D. Shirley, *Rev. Mod. Phys.*, 1964, **36**, 339.
13 *Mössbauer Isomer Shifts*, ed. G. K. Shenoy and F. E. Wagner, North-Holland, Amsterdam, 1978.
14 M. Filatov, *Coord. Chem. Rev.*, 2009, **253**, 594–605.
15 J. Cederberg, D. Olson, J. Larson, G. Rakness, K. Jarausch, J. Schmidt, B. Borovsky, P. Larson and B. Nelson, *Phys. Rev. A*, 1998, **57**, 2539–2543.
16 J. Cederberg, J. Nichol, E. Frodermann, H. Tollerud, G. Hilk, J. Buysman, W. Kleiber, M. Bongard, J. Ward, K. Huber, T. Khanna, J. Randolph and D. Nitz, *J. Chem. Phys.*, 2005, **123**, 134321.
17 G. Paquette, A. Kotz, J. Cederberg, D. Nitz, A. Kolan, D. Olson, K. Gunderson, S. Lindaas and S. Wick, *J. Mol. Struct.*, 1988, **190**, 143–148.
18 J. Cederberg, J. Randolph, B. McDonald, B. Paulson and C. McEachern, *J. Mol. Spectrosc.*, 2008, **250**, 114.
19 J. Cederberg, E. Frodermann, H. Tollerud, K. Huber, M. Bongard, J. Randolph and D. Nitz, *J. Chem. Phys.*, 2006, **124**, 244304.
20 J. Cederberg, S. Fortman, B. Porter, M. Etten, M. Feig, M. Bongard and L. Langer, *J. Chem. Phys.*, 2006, **124**, 244305.
21 J. Cederberg, B. Paulson and C. Conklin, *J. Mol. Spectrosc.*, 2011, **265**, 92.
22 A. Lesarri, R. D. Suenram and D. Brugh, *J. Chem. Phys.*, 2002, **117**, 9651.
23 S. A. Cooke and M. C. L. Gerry, *J. Mol. Spectrosc.*, 2002, **216**, 122–130.
24 S. G. Kukolich and S. M. Sickafoose, *J. Chem. Phys.*, 1993, **99**, 6465.
25 B. J. Drouin, P. A. Cassak and S. G. Kukolich, *J. Chem. Phys.*, 1998, **108**, 8878.
26 C. Stoeffler, B. Darquie, A. Shelkovnikov, C. Daussy, A. Amy-Klein, C. Chardonnet, L. Guy, J. Crassous, T. R. Huet, P. Soulard and P. Asselin, *Phys. Chem. Chem. Phys.*, 2011, **13**, 854–863.
27 P. Pyykkö, *J. Phys. F: Met. Phys.*, 1971, **1**, 102.

